

# Circuit Model Extraction of Parallel-Connected Dual-Passband Coupled-Resonator Filters

Ping Zhao<sup>1</sup>, *Student Member, IEEE*, and Ke-Li Wu<sup>2</sup>, *Fellow, IEEE*

**Abstract**—In this paper, an analytical coupling matrix extraction scheme is proposed for parallel-connected dual-passband coupled-resonator filters for the first time. Model-based vector fitting technique is adopted to fit the measured responses of the dual-passband filter (DPBF) with a set of rational functions, from which a transversal coupling matrix can be constructed. A novel coupling matrix transformation strategy is developed to transform the transversal coupling matrix to the one corresponding to the topology of a parallel-connected DPBF. A practical filter is used as a test example to demonstrate the extraction procedure. In diagnosing the coupling matrix of the test filter, two kinds of ambiguity problems are discussed in detail and are solved by a perturbation technique. This paper provides a general theoretic framework for computer-aided tuning of a parallel-connected dual-passband or multiple-passband filter.

**Index Terms**—Computer-aided tuning (CAT), coupling matrix, dual-band filter, rational approximation, vector fitting (VF).

## I. INTRODUCTION

TUNING a narrowband coupled-resonator device, such as a filter or a diplexer, is a necessary but challenging task due to the conflict between the stringent requirement on its frequency response and the low-cost and loosely controlled manufacture precision. To prepare an advanced automatic tuning system using a robotic arm, researchers have paid a great deal of effort on investigating efficient computer-aided tuning (CAT) algorithms. Among all the existing methods, analytic diagnosis techniques that do not rely on initial values and time-consuming optimization will be promising choices for a potential real-time robotic tuning system. Toward this end, several deterministic techniques have already been proposed for coupled-resonator single-band filters [1]–[3], and diplexers [4].

As the frequency spectrum gets more and more crowded, dual-passband filters (DPBFs) are also finding more and more applications where the allocated spectrum contains two non-continuous bands. Applications of DPBFs include interference mitigation filters and multiband combiners. For a practical DPBF design, independent controls of filtering response and

coupling topology of each channel filter are desirable. Additionally, the convenience in realizing the layout of coupled resonators is also an important factor in the design. Taking these concerns into account, the most practical option for a practical industry application is the parallel-connected DPBF, where the response and the coupling topology of each channel filter can be independently controlled with good flexibility. In recent years, attentions have been given to the synthesis theory of DPBFs [5]–[7]. However, the CAT algorithm for such an important species of filters has not been studied.

The model-based vector fitting (MVF) is a rational approximation technique proposed for analytically extracting the characteristic functions of a coupled-resonator diplexer from its measured responses [4], which is evolved from the vector fitting (VF) method [8]. While retaining the iterative pole relocation procedure of original VF for accurately determining the system poles, MVF possesses the unique feature of capable of stipulating the number of transmission zeros (TZs) of rational system functions. This property allows accurately recovering of the filtering function of a coupled-resonator network when the interference of measurement noise is significant. In this paper, MVF is adopted for the extraction of the characteristic functions of a parallel-connected DPBF from the measured data, from which the circuit model of a DPBF can be constructed. Specifically, the circuit model will be represented by a coupling matrix in the given coupling topologies of two channel filters and two common resonator combining junctions. A generic and novel coupling matrix reconfiguration procedure is developed, which transforms the coupling matrix in the transversal form to the one complying with the physical coupling layout of the parallel-connected DPBF under tuning.

The theory and the general extraction process are illustrated by a CAT example of a parallel-connected DPBF. Fig. 1 shows the photograph of a filter bank module that consists of four parallel-connected DPBFs, one of which will be used as the test filter for the tuning example. For the test filter, the lower passband is 1884.5–1915.5 MHz and the upper passband is 2009–2026 MHz. The coupling routing diagram of the filter is shown in Fig. 2. It can be seen that the upper band filter has four resonators in a direct-coupled structure and the lower band filter has eight resonators in a cascaded tri-section (CT) structure. The two channel filters are combined by common resonator junctions at both ends.

Although only one specific filter is discussed in detail, the rational function approximation formulation, the coupling

Manuscript received April 6, 2017; revised July 25, 2017 and August 29, 2017; accepted September 30, 2017. Date of publication October 31, 2017; date of current version February 5, 2018. This work was supported by the Postgraduate Studentship of The Chinese University of Hong Kong. (Corresponding author: Ping Zhao.)

The authors are with the Department of Electronic Engineering, The Chinese University of Hong Kong, Hong Kong (e-mail: aoiing56@gmail.com; kluwu@ee.cuhk.edu.hk).

Color versions of one or more of the figures in this paper are available online at <http://ieeexplore.ieee.org>.

Digital Object Identifier 10.1109/TMTT.2017.2764086

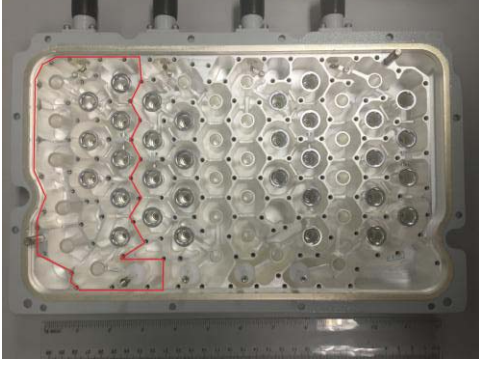


Fig. 1. Hardware of the test DPBF with top lid removed. There are four filters in the same coupling topology and with the same specifications. Measured data of the one on the left-hand side highlighted with red borders are used to demonstrate the coupling matrix extraction procedure.

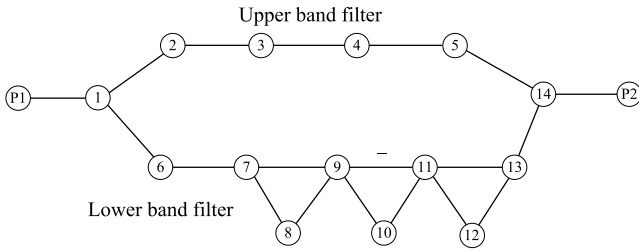


Fig. 2. Routing diagram of the test DPBF. Hollow circles with numbers inside are resonators. Solid lines represent couplings.

matrix transformation strategy and the perturbation method for solving multiple-solution problem introduced in this paper can be easily generalized to other parallel-structured DPBFs realized in different coupling topologies.

## II. EXTRACTION OF CHARACTERISTIC FUNCTIONS

### A. Phase Correction

Once the frequency-domain responses of the DPBF are measured, the physical frequency  $f$  is first mapped to the low-pass domain by

$$\omega = \frac{f_0}{BW} \left( \frac{f}{f_0} - \frac{f_0}{f} \right). \quad (1)$$

The complex frequency variable  $s = j\omega$  is used in the characteristic functions. For the test filter,  $f_0$  and  $BW$  are chosen to be 1954 and 141.5 MHz, respectively.

In order to obtain the scattering parameters corresponding to the coupled-resonator network, the phase loading and transmission line at each port should be de-embedded [1] to make the phase responses asymptotically tend to zero. For example, of one tuning state, the measured phases of the reflection coefficients at the two ports are shown in Fig. 3(a). The corrected phases are shown in Fig. 3(b). Then the processed S-parameters are converted to Y-parameters with unitary reference admittance at both ports to prepare for the extraction of poles and residues of the characteristic functions.

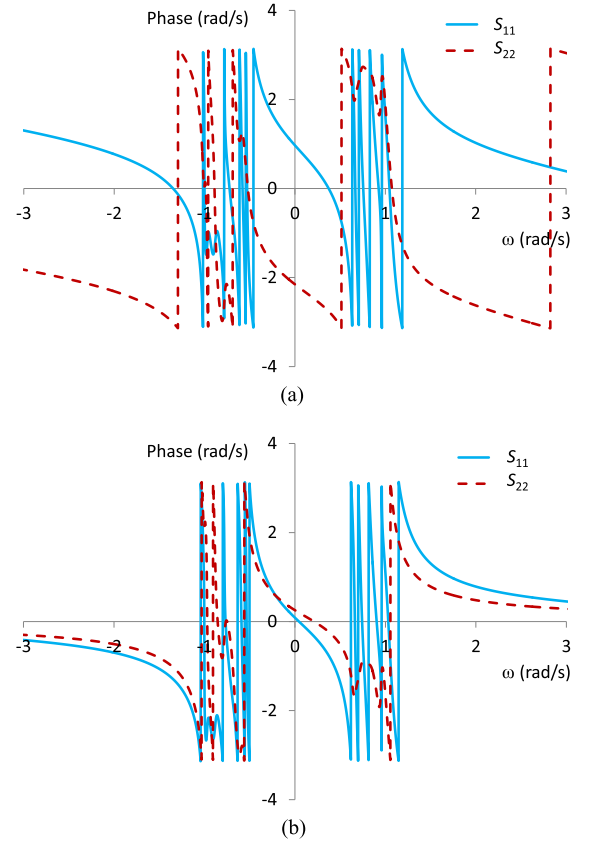


Fig. 3. (a) Phases of the raw measured reflection coefficients at both ports. (b) Phases of the reflection coefficients after de-embedding of phase loading and transmission line effects.

### B. Formulating MVF Equations

From the routing diagram in Fig. 2, it can be seen that there are 14 resonators in the filter network, and the shortest path from Port 1 to Port 2 is P1-1-2-3-4-5-14-P2, passing through six resonators. Thus, there are 14 dominant poles and eight zeros in the transadmittance function  $Y_{12}$  according to the *minimum path rule* [9]. MVF fits the short-circuit admittance functions in the following form [4]

$$[\mathbf{Y}] = \frac{1}{\sum_{k=1}^{14} \frac{\tilde{c}_k}{s - a_k} + 1} \begin{bmatrix} \sum_{k=1}^{14} \frac{c_k^{11}}{s - a_k} + d^{11} & \frac{\sum_{k=0}^8 c_k^{12} s^k}{\prod_{k=1}^{14} (s - a_k)} \\ \frac{\sum_{k=0}^8 c_k^{12} s^k}{\prod_{k=1}^{14} (s - a_k)} & \sum_{k=1}^{14} \frac{c_k^{22}}{s - a_k} + d^{22} \end{bmatrix}. \quad (2)$$

The common poles  $a_k$ , and the coefficients  $c$  and  $d$  in (2) are determined to minimize the residual between the rational function and the measured data in the sense of least squares (LS).

In practice, the number of TZs detected can be different from that determined by the minimum path rule due to

parasitic couplings. Setting inappropriate number of TZs may lead to a poor fitting result and failure in transforming the coupling matrix to the one with the desired topology. A good practice is to use the theoretical number of TZs first, and if the fitting does not give a satisfactory result, a slightly higher order for the numerator can be used. In this example, the order of transadmittance function agrees with the theoretical result.

By MVF, the numerator order of  $Y_{12}$  is enforced to be 8 in (2), which corresponds to the eight zeros in the transfer function. The system equations are formulated as

$$\begin{bmatrix} \mathbf{A}_1 & \mathbf{0} & \mathbf{0} & -\mathbf{Y}_{11}\mathbf{A}_2 \\ \mathbf{0} & \mathbf{W}_{12}\mathbf{A}_3 & \mathbf{0} & -\mathbf{W}_{12}\mathbf{Y}_{12}\mathbf{A}_2 \\ \mathbf{0} & \mathbf{0} & \mathbf{A}_1 & -\mathbf{Y}_{22}\mathbf{A}_2 \end{bmatrix} \begin{bmatrix} \mathbf{c}_{11} \\ \mathbf{c}_{12} \\ \mathbf{c}_{22} \\ \tilde{\mathbf{c}} \end{bmatrix} = \begin{bmatrix} \mathbf{y}_{11} \\ \mathbf{W}_{12}\mathbf{y}_{12} \\ \mathbf{y}_{22} \end{bmatrix} \quad (3)$$

where

the  $i$ -th row of

$$\mathbf{A}_1 = \begin{bmatrix} 1 & 1 & \cdots & 1 & 1 \end{bmatrix}$$

$$\mathbf{A}_1 \in \mathbb{C}^{m \times 15} \quad (4)$$

the  $i$ -th row of

$$\mathbf{A}_2 = \begin{bmatrix} 1 & 1 & \cdots & 1 \end{bmatrix}$$

$$\mathbf{A}_2 \in \mathbb{C}^{m \times 14} \quad (5)$$

the  $i$ -th row of

$$\mathbf{A}_3 = \begin{bmatrix} 1 & s_i & \cdots & s_i^8 \end{bmatrix}$$

$$\mathbf{A}_3 \in \mathbb{C}^{m \times 9} \quad (6)$$

$$\mathbf{Y}_{pq} = \text{diag}\{Y_{pq}(s_i)\} \in \mathbb{C}^{m \times m} \quad (7)$$

$$\mathbf{y}_{pq} = [Y_{pq}(s_1) \cdots Y_{pq}(s_m)]^T \in \mathbb{C}^{m \times 1} \quad (8)$$

$$\mathbf{W}_{12} = \text{diag}\{1/\sqrt{|Y_{12}(s_i)|}\} \in \mathbb{R}^{m \times m} \quad (9)$$

$$\mathbf{c}_{pp} = [c_1^{pp} \ c_2^{pp} \ \cdots \ c_{14}^{pp} \ d^{pp}]^T \in \mathbb{C}^{15 \times 1} \quad (10)$$

$$\mathbf{c}_{12} = [c_0^{12} \ c_1^{12} \ \cdots \ c_7^{12} \ c_8^{12}]^T \in \mathbb{C}^{9 \times 1} \quad (11)$$

$$\tilde{\mathbf{c}} = [\tilde{c}_1 \ \tilde{c}_2 \ \cdots \ \tilde{c}_{14}]^T \in \mathbb{C}^{14 \times 1} \quad (12)$$

and  $m$  is the total number of sampled frequency points.

In (3), there are three block rows for fitting  $Y_{11}$ ,  $Y_{12}$ , and  $Y_{22}$ , respectively, and making them share common poles. In (4)–(12),  $\mathbf{A}_1$  and  $\mathbf{A}_2$  are the system matrices with partial fractions as the basis functions for fitting  $Y_{11}$  and  $Y_{22}$ .  $\mathbf{A}_3$  is the matrix with pole-located monomials as the basis functions for fitting  $Y_{12}$ , whose order is up to 8 as determined by the number of TZs of the filter.  $\mathbf{W}_{12}$  holds the weighting factors in fitting  $Y_{12}$  to balance the contribution of data with large and small magnitude. Indices  $p$  and  $q$  are 1 or 2.  $Y_{pq}(s_i)$  are the measured data of  $Y_{pq}$  at frequency  $s_i$ .

In order to ensure good conditioning of the system matrix (3), the 14 initial poles  $a_k$  are chosen as complex numbers whose imaginary parts are linearly distributed in the

interval  $[-1 \ 1.1]$  and real parts are all negative with absolute values of 1% of the imaginary parts.

After (3) is solved in the sense of LS, the poles  $a_k$  are relocated to the loci of the zeros of

$$\sum_{k=1}^{14} \frac{\tilde{c}_k}{s - a_k} + 1 = 0 \quad (13)$$

which can be computed as the eigenvalues of the following matrix [10]

$$\mathbf{A} - \mathbf{b} \cdot \tilde{\mathbf{c}}^T \quad (14)$$

where  $\mathbf{A}$  is a diagonal matrix holding the original poles  $a_k$ , and  $\mathbf{b}$  is a column vector whose entries are ones. With the updated poles, (3) is reformulated and solved iteratively until the loci of the poles are stable and  $\tilde{\mathbf{c}} = \mathbf{0}$ .

### C. Fast Solution

It can be seen from (14) that in the *iterative pole relocation* procedure only  $\tilde{\mathbf{c}}$  is involved for computing new poles, whereas  $\mathbf{c}_{11}$ ,  $\mathbf{c}_{12}$ , and  $\mathbf{c}_{22}$  are not used. By taking advantage of the so-called *bordered block diagonal* structure of (3), a fast algorithm is possible [11]. Note that one block row of (3) is in the form of

$$[\Phi_1 \ -\mathbf{Y}_{pq}\Phi_2] \begin{bmatrix} \mathbf{c}_{pq} \\ \tilde{\mathbf{c}} \end{bmatrix} = \mathbf{y}_{pq}. \quad (15)$$

First compute the thin QR factorization of  $[\Phi_1 \ -\mathbf{Y}_{pq}\Phi_2]$  as

$$[\Phi_1 \ -\mathbf{Y}_{pq}\Phi_2] = \underbrace{[\mathbf{Q}_{pq}^{11} \ \mathbf{Q}_{pq}^{12}]}_{\mathbf{Q}_{pq}} \underbrace{\begin{bmatrix} \mathbf{R}_{pq}^{11} & \mathbf{R}_{pq}^{12} \\ \mathbf{0} & \mathbf{R}_{pq}^{22} \end{bmatrix}}_{\mathbf{R}_{pq}}. \quad (16)$$

In (16),  $\mathbf{Q}_{pq}$  is a “tall and thin” matrix with orthonormal columns and  $\mathbf{R}_{pq}$  is an upper triangular matrix. Multiplying both sides of (15) on the left by  $\mathbf{Q}_{pq}^H$  yields

$$\begin{bmatrix} \mathbf{R}_{pq}^{11} & \mathbf{R}_{pq}^{12} \\ \mathbf{0} & \mathbf{R}_{pq}^{22} \end{bmatrix} \begin{bmatrix} \mathbf{c}_{pq} \\ \tilde{\mathbf{c}} \end{bmatrix} = \begin{bmatrix} \mathbf{Q}_{pq}^{11H} \\ \mathbf{Q}_{pq}^{12H} \end{bmatrix} \mathbf{y}_{pq}. \quad (17)$$

The second block row of (17) can be collected for all three block rows of (3) to obtain the following over-determined equations for  $\tilde{\mathbf{c}}$

$$\begin{bmatrix} \mathbf{R}_{11}^{22} \\ \mathbf{R}_{12}^{22} \\ \mathbf{R}_{22}^{22} \end{bmatrix} \tilde{\mathbf{c}} = \begin{bmatrix} \mathbf{Q}_{11}^{12H} \\ \mathbf{Q}_{12}^{12H} \\ \mathbf{Q}_{22}^{12H} \end{bmatrix} \mathbf{y}_{pq} \quad (18)$$

$\tilde{\mathbf{c}}$  is solved from (18) and used in (14) to compute new poles. When  $\tilde{\mathbf{c}}$  approaches to a zero vector, the iterative procedure converges and the optimal loci of all the poles  $a_k$  are known. Then  $\mathbf{c}_{11}$ ,  $\mathbf{c}_{12}$ , and  $\mathbf{c}_{22}$  can be determined by another LS formulation

$$\mathbf{A}_1 \mathbf{c}_{11} = \mathbf{y}_{11} \quad \mathbf{W}_{12} \mathbf{A}_3 \mathbf{c}_{12} = \mathbf{W}_{12} \mathbf{y}_{12} \quad \mathbf{A}_1 \mathbf{c}_{22} = \mathbf{y}_{22} \quad (19)$$

where all the matrices above are defined in (4)–(12).

For one tuning state of the test filter, the measured data and fit rational functions of Y-parameters are shown in Fig. 4(a) and (b) with logarithmic scale. It can be seen that very good agreement is achieved.

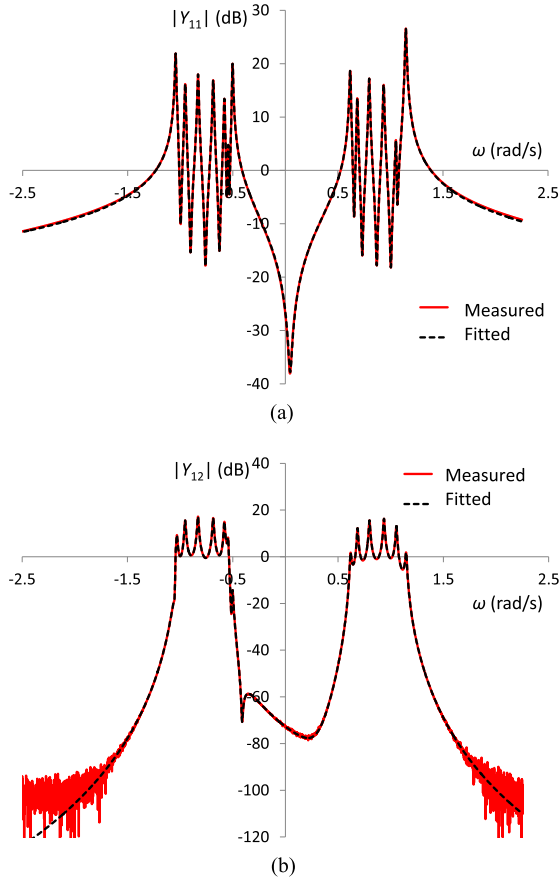


Fig. 4. (a) Measured and fitted  $Y_{11}$  by MVF. (b) Measured and fitted  $Y_{12}$  by MVF.

#### D. Construction of Transversal Coupling Matrix

The fitting results of  $Y_{11}$  and  $Y_{22}$  are already in the pole-residue form. The rational function  $Y_{12}$  obtained by MVF has to be transformed to the pole-residue form to be prepared for synthesizing the lossy transversal coupling matrix [12]. The  $Y$ -matrix in pole-residue form is

$$[\mathbf{Y}] = \begin{bmatrix} K_{11} & 0 \\ 0 & K_{22} \end{bmatrix} + \sum_{k=1}^{14} \frac{1}{s - p_k} \begin{bmatrix} r_{11}^k & r_{12}^k \\ r_{12}^k & r_{22}^k \end{bmatrix}. \quad (20)$$

However, the compact residue condition

$$r_{11}^k r_{22}^k = r_{12}^k r_{12}^k \quad (21)$$

is not enforced by the rational fitting process, thus the following strategy is adopted to construct the complex transversal coupling matrix for the filter

for  $k = 1$  to  $N$

$$M_{k,k} = j * p_k$$

$$\text{if } |r_{11}^k| \geq |r_{22}^k|$$

$$M_{P1,k} = \sqrt{r_{11}^k} \quad M_{P2,k} = r_{12}^k / \sqrt{r_{11}^k}$$

$$\text{elseif } |r_{22}^k| > |r_{11}^k|$$

$$M_{P2,k} = \sqrt{r_{22}^k} \quad M_{P1,k} = r_{12}^k / \sqrt{r_{22}^k}$$

end

$$M_{k,P1} = M_{P1,k} \quad M_{k,P2} = M_{P2,k}$$

end

$$M_{P1,P1} = K_{11}/j \quad M_{P2,P2} = K_{22}/j$$

where  $j$  stands for the imaginary unit in a complex number.

### III. GENERAL TRANSFORMATION STRATEGY

The transversal coupling matrix cannot guide the tuning of the filter. It has to be transformed to the right form corresponding to the routing diagram of resonators in the physical realization, in which one-to-one correspondence between entries in the coupling matrix and physical tuning elements is established.

Similarity transformation, which is used to reduce the  $N+2$  transversal coupling matrix to the form corresponding to the physical realization, takes the form of

$$\mathbf{M}' = \mathbf{R}\mathbf{M}\mathbf{R}^{-1}. \quad (22)$$

In order to obtain a symmetric matrix  $\mathbf{M}'$ , the matrix  $\mathbf{R}$ , either real or complex, must satisfy

$$\mathbf{R}\mathbf{R}^T = \mathbf{I} \quad (23)$$

where  $\mathbf{I}$  is the identity matrix and superscript  $T$  denotes matrix transpose. If the first and last nodes in  $\mathbf{M}$  represent the two ports of the filter, in order to preserve the transfer and reflection characteristics, the matrix  $\mathbf{R}$  must be in the form of

$$\mathbf{R} = \begin{bmatrix} 1 & \mathbf{0} & 0 \\ \mathbf{0} & \mathbf{R}_{\text{core}}^{N \times N} & \mathbf{0} \\ 0 & \mathbf{0} & 1 \end{bmatrix} \quad (24)$$

where all the outermost entries of  $\mathbf{R}$  are 0 except that the top-left and bottom-right elements are 1.

Conventional transformation strategies adopt rotation matrices  $\mathbf{R}$  where each of them can be uniquely specified by a pivot  $(i, j)$  and a rotation angle  $\theta_r$  [13]. Usually one unwanted coupling in the coupling matrix is annihilated by applying transformation (22) once. In the transformation procedure to be introduced, the matrix  $\mathbf{R}$  also adopts other kinds of matrices which also satisfy (23) and (24).

The transformation procedure for the parallel-connected DPBF can be divided into three steps, which are illustrated in Fig. 5(a)–(e), where hollow circles represent expected nonzero entries at each stage in an ideal case. The sequence of resonators is indicated in Fig. 2.

*Step 1:* The nonexistent I/O couplings in the outermost rows and columns of the  $N+2$  transversal coupling matrix in Fig. 5(a) are annihilated one-by-one with rotation matrices  $\mathbf{R}$ , leading to two I/O couplings left that correspond to the physical I/O couplings connecting the ports to the first and last resonators, respectively. The resultant matrix of this step has a nearly full  $N$ -by- $N$  core submatrix, as shown in Fig. 5(b).

*Step 2:* The core  $N$ -by- $N$  submatrix is transformed to a transversal form, as shown in Fig. 5(c). This transformation is accomplished by the diagonalization of the core

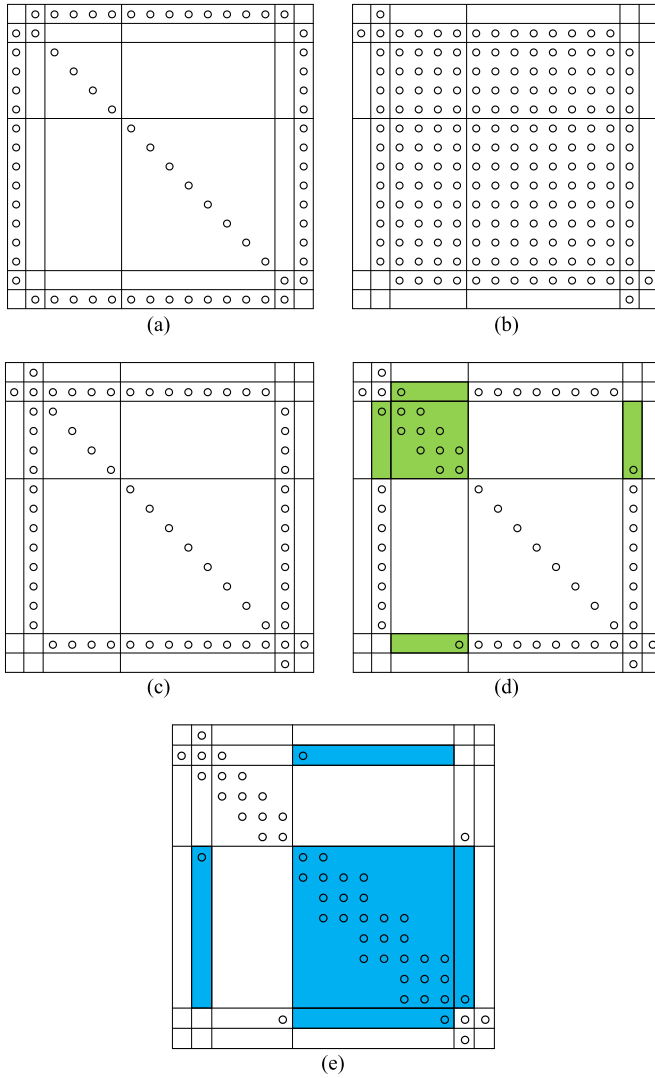


Fig. 5. Proposed transformation procedure. (a) Transversal coupling matrix. (b) After annihilating non-existing I/O couplings. (c) Core  $(N-2) \times (N-2)$  submatrix is diagonalized. (d) Upper band filter is transformed to the right form. (e) Lower band filter is transformed to the right form and the final coupling matrix corresponding to the physical realization.

$(N-2)$ -by- $(N-2)$  submatrix. Let the coupling matrix after step 1 be written in block matrices as

$$\mathbf{M} = \begin{bmatrix} \mathbf{M}_{11}^{2 \times 2} & \mathbf{M}_{12}^{2 \times (N-2)} & \mathbf{M}_{13}^{2 \times 2} \\ \mathbf{M}_{21}^{(N-2) \times 2} & \mathbf{M}_{22}^{(N-2) \times (N-2)} & \mathbf{M}_{23}^{(N-2) \times 2} \\ \mathbf{M}_{31}^{2 \times 2} & \mathbf{M}_{32}^{2 \times (N-2)} & \mathbf{M}_{33}^{2 \times 2} \end{bmatrix} \quad (25)$$

where the superscripts denote the dimensions of corresponding submatrices and will be dropped in the following discussion.

Compute the spectral decomposition of the core submatrix  $\mathbf{M}_{22}$

$$\mathbf{M}_{22} = \mathbf{V} \mathbf{\Lambda} \mathbf{V}^{-1} \quad (26)$$

where  $\mathbf{\Lambda}$  is a diagonal matrix holding the eigenvalues of  $\mathbf{M}_{22}$  and each column of  $\mathbf{V}$  is an eigenvector of  $\mathbf{M}_{22}$ . For a lossless network,  $\mathbf{M}_{22}$  is real and symmetric, thus  $\mathbf{V}$  is an orthogonal

matrix and the rotation matrix  $\mathbf{R}$  can be constructed as

$$\mathbf{R} = \begin{bmatrix} \mathbf{I} & \mathbf{0} & \mathbf{0} \\ \mathbf{0} & \mathbf{V}^{-1} & \mathbf{0} \\ \mathbf{0} & \mathbf{0} & \mathbf{I} \end{bmatrix} \quad (27)$$

where  $\mathbf{I}$  denotes the  $2 \times 2$  identity matrix. It can be seen that  $\mathbf{R}$  is also an orthogonal matrix. By the similarity transformation (22), one can readily obtain the coupling matrix in the form of Fig. 5(c).

In reality, however, all filters dissipate power to certain degree and their coupling matrices have complex entries. Thus, the lossless case is not applicable to diagnosed coupling matrices; since for complex matrices, the spectral decomposition (26) does not lead to an orthogonal matrix  $\mathbf{V}$  in general. It can be shown that for a generic complex and symmetric matrix  $\mathbf{M}_{22}$  with its spectral decomposition (26), matrix  $\mathbf{V}$  satisfies [14]

$$\mathbf{V}^T \mathbf{V} = \mathbf{D} \quad (28)$$

where  $\mathbf{D}$  is a diagonal matrix with complex entries. Then the rotation matrix  $\mathbf{R}$  can be constructed by

$$\mathbf{R} = \begin{bmatrix} \mathbf{I} & \mathbf{0} & \mathbf{0} \\ \mathbf{0} & \mathbf{D}^{1/2} \mathbf{V}^{-1} & \mathbf{0} \\ \mathbf{0} & \mathbf{0} & \mathbf{I} \end{bmatrix} \quad (29)$$

where  $\mathbf{D}^{1/2}$  denotes a diagonal matrix, whose entries are square roots of corresponding entries in  $\mathbf{D}$ . It can be verified that (23) is satisfied by the  $\mathbf{R}$  in (29). The transformed matrix  $\mathbf{M}'$  obtained by (22) can reserve the coupling values of the outermost elements of the matrix and at the same time leads to a diagonal core  $(N-2) \times (N-2)$  submatrix. This matrix structure corresponds to  $N-2$  parallel paths between the two end resonators of the filter.

*Step 3:* The routing diagram of the coupling matrix in Fig. 5(c) is illustrated by Fig. 6(a). In the last step, the lower and upper band filters are transformed separately like two individual filters. The coupling matrices in Fig. 5(d) and (e) illustrate two sequential operations to transform the upper and lower band filters, respectively, where the blocks with colored background denote the upper and lower band filters. Each of the blocks can be reconfigured independently using those well-established transformation recipes for single-band filters in [13]. In this step, the coupling topology is transformed from the one in Fig. 6(a) to that in Fig. 6(b).

The difficulty in implementing the third step lies in how to identify the association of the nodes in the core  $(N-2)$ -by- $(N-2)$  submatrix with the lower and upper band filters. For a tuning state where the upper and lower band characteristics are well separated in spectrum, the association can be determined by the real parts of diagonal entries in the core  $(N-2)$ -by- $(N-2)$  submatrix in Fig. 5(c). For a more general case, perturbation on some frequency tuning screws will be an effective approach, as will be demonstrated in the next section.

After partition of the nodes is done, since the two branches are in their transversal forms, as shown in the dashed line boxes in Fig. 6(a), the rational functions of  $Y$ -parameters of the two branch filters can be obtained by the reverse

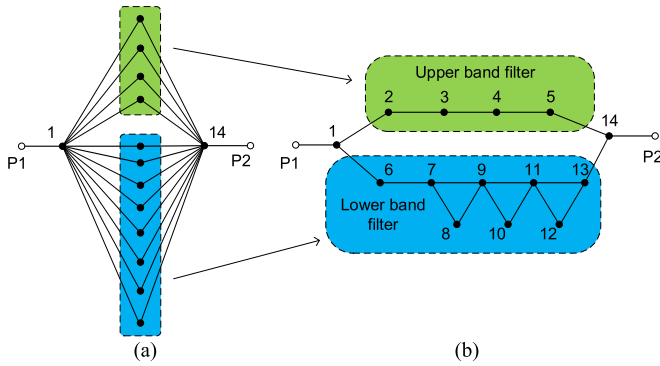


Fig. 6. Coupling topologies of a dual-band parallel-connected filter in (a) canonical form of block transversal coupling topology corresponding to matrix form of Fig. 5(c). (b) Physical coupling topology corresponding to matrix form of Fig. 5(e).

procedure of coupling matrix synthesis. Then the TZs of the two branches can be analytically founded by computing the zeros of their  $Y_{12}$  rational functions, whose values will take part in subsequent matrix transformations.

The idea of presented transformation scheme is general for parallel-connected DPBFs, where each parallel path can be with different coupling topologies. The procedure presented in Fig. 5(a)–(e) is for the illustrative example of the 14–8 filter in Fig. 1. After proper repartition of the nodes, the transformation procedure should lead to the desired circuit form because the measured data come from the physical filter realized in the coupling topology of Fig. 6(b). Note that for general 14–8 filters in synthesis problems, the presented transformation scheme is usually not able to produce such parallel structure.

IV. PERTURBATION METHOD

For a general parallel-connected DPBF combined by common resonator junctions at both ends, in performing the matrix transformation strategy proposed in the last section, two kinds of ambiguity need to be solved: 1) the association of nodes with the single-band filters and 2) the association of TZs with the cascaded coupling structure, where multiple-resolution problem exists. Both kinds of ambiguity can be solved by perturbation on the concerned tuning screw, as will be explained in this section.

A. Perturbation for Solving the First Kind of Ambiguity

For one tuning state of the test filter, the measured data and the responses of the fitting model are shown in Fig. 7(a). The extracted coupling matrix has been transformed to the form of Fig. 5(c). In order to proceed with the coupling matrix transformation procedure, one must decide which parallel nodes belong to the lower band filter and which belong to the upper band filter.

A simple method is to partition the nodes according to the real parts of the diagonal entries as smaller real parts correspond to higher resonant frequencies. This method can be applied if the transfer characteristics of the two passbands are well-separated in spectrum. However, in Fig. 7(a), the transfer

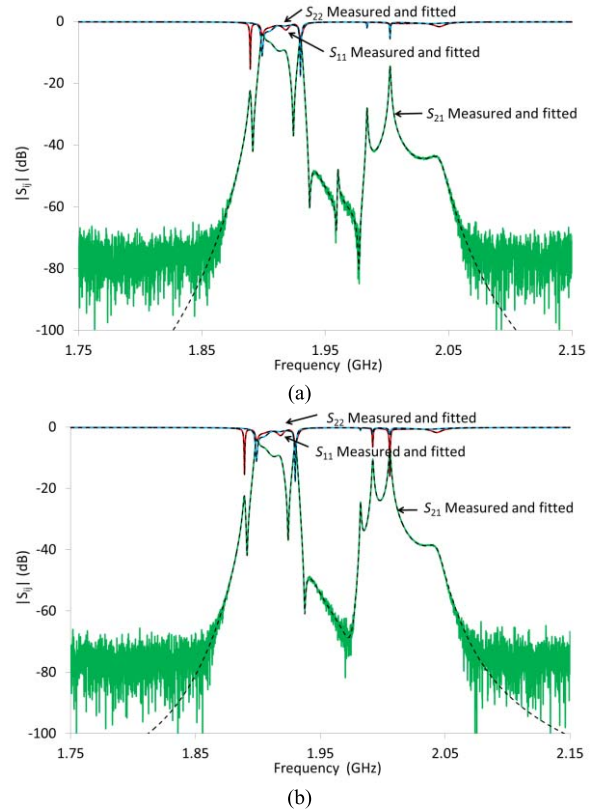


Fig. 7. (a) Measured and model fitted responses before perturbation. (b) Measured and fitted responses after perturbation on resonator number 3. Dashed lines are responses of extracted coupling matrix. Solid lines are raw measured data.

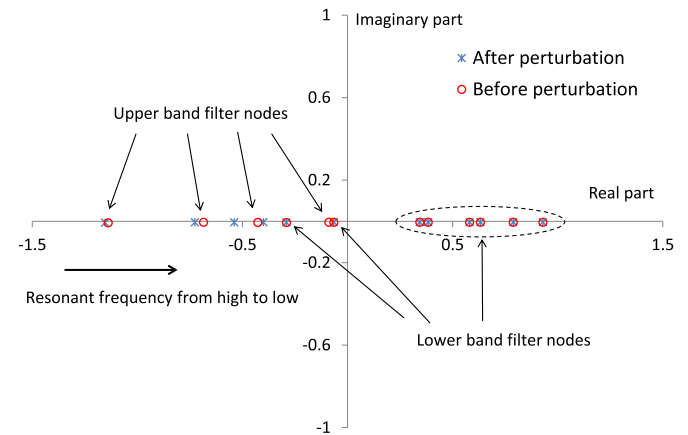


Fig. 8. Diagonal entries of the extracted coupling matrix in the form of Fig. 5(c) corresponding to the tuning states in Fig. 7 before and after perturbation on resonator number 3.

characteristics of the two single-band filters cannot be clearly distinguished from each other. Thus perturbation is conducted to solve the ambiguity.

Only the tuning screw controlling the resonant frequency of resonator number 3 is perturbed. The resultant responses are shown in Fig. 7(b). Repeating the coupling matrix extraction procedure, one can obtain another coupling matrix corresponding to the perturbed state. Since the lower band filter has not changed, the couplings and resonant frequencies of the nodes

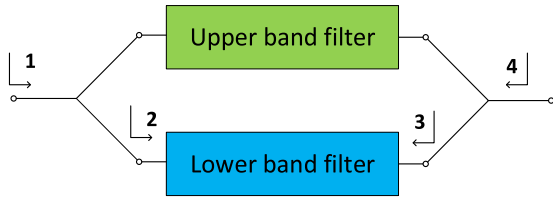


Fig. 9. Parallel-connected DPBF structure.

belonging to the lower band filter should be no different except for some small numerical errors. The four eigenvalues and the associated couplings of the upper band nodes are all changed since all the poles and residues of the upper band filter are affected by the perturbation on resonator number 3.

The 12 diagonal entries from  $M_{22}$  to  $M_{13,13}$  of the two extracted coupling matrices in the form of Fig. 5(c) before and after the perturbation are shown in the complex plane in Fig. 8. All the entries have small imaginary parts, and thus locate very close to the real axis. Obviously after the perturbation on resonator number 3, four of the diagonal entries are changed; whereas, other eight nodes stand still. Now one can readily tell the four nodes belonging to the upper band filter from the other eight nodes.

Once the attribution of the nodes has been decided, one can use a suitable permutation matrix  $\mathbf{R}$  in (22) to reorder the sequence of the nodes to put the nodes belonging to the upper band filter ahead of those of the lower band filter. The regrouping of the nodes is critical to obtain the right solution but the sequence of the nodes in each band filter has no effect on the final coupling matrix obtained by subsequent transformations.

### B. Perturbation for Solving the Second Kind of Ambiguity

After the sequence of nodes is sorted, the two filters can be reconfigured separately, as illustrated by Fig. 6(a) and (b). In the upper band filter, the four resonators are in a direct cascaded form, which can be obtained without ambiguity. In the lower band filter, the eight resonators are arranged in a CT form realizing three TZs on the imaginary axis. Note that in the parallel-connected structure, the three TZs of the lower band filter are different from the eight TZs of the DPBF. This is a distinct feature of the parallel structure as signals blocked by one path can still be passed through the other path. As shown in Fig. 9, the TZs between nodes 1 and 4 are different from those seen between nodes 2 and 3. To address the multiple-solution problem of the lower band filter, the TZs discussed in this section and listed in Table I are referring to the TZs of the lower band filter, i.e., between locations 2 and 3 in Fig. 9.

It is well-known that a tri-section contributes a single TZ on the imaginary axis in a single-path filter. In order to reach the CT form, each TZ must be associated with one tri-section because the rotation angle of matrix  $\mathbf{R}$  in (22) is related to the locus of the assigned TZ [15]. Different TZ assignments lead to solutions of different resultant coupling matrices. In [16], the multiple-solution problem in a cascaded quartet filter design is solved by computing all possible solutions and picking out the one with minimum extra couplings. In this

TABLE I  
COMPUTED TZS OF THE LOWER BAND FILTER FROM EXTRACTED COUPLING MATRICES BEFORE AND AFTER PERTURBATION ON RESONATOR NUMBER 8

	TZ <sub>1</sub>	TZ <sub>2</sub>	TZ <sub>3</sub>	TZ <sub>4</sub>
Before	-0.0046	-0.0043	-0.0049	-0.0484
perturbation	-0.3172i	-0.5136i	-0.9179i	+8.1925i
After	-0.0047	-0.0043	-0.0049	-0.0512
perturbation	-0.4106i	-0.5137i	-0.9182i	+8.1553i

paper, a different approach, i.e., perturbation on a few relevant resonators is adopted to find the true association of the TZs.

To find out which TZ is contributed by the tri-section constructed by resonators number 7 through 9, perturbation on resonator number 8 can be performed. After the extracted coupling matrix has been transformed to the form of Fig. 5(c) and the nodes belonging to the lower and upper band filters have been sorted, the lower band filter block matrix on the lower-right corner of Fig. 5(c) is in a transversal form. Then the  $Y$ -parameters rational functions pertinent to the lower band filter can be readily obtained in a pole-residue form by the reverse procedure of transversal coupling matrix synthesis. The TZs of the lower band filter can be computed as the zeroes of obtained  $Y_{12}$  rational function.

Theoretically there should be three TZs on the imaginary axis as a result of the three tri-sections. Due to dispersion, power dissipation, parasitic couplings, and other imperfections of the filter, four complex TZs are actually diagnosed, as shown in Table I. Obviously TZ<sub>4</sub> is beyond the frequency range of interest and can be attributed to the aggregated nonideal effects. Only TZ<sub>1</sub> through TZ<sub>3</sub> are created by the three tri-sections in the lower band filter.

After slightly perturbing the tuning screw which controls the resonant frequency of resonator number 8 and keeping all the other tuning screws unchanged, repeating the above procedure yields the new loci of TZs. The TZs after the perturbation are listed in the third row of Table I. By comparing the loci of TZs before and after the perturbation, one can readily tell TZ<sub>1</sub> is created by the tri-section composed of resonators number 7 through 9. TZ associations of the other two tri-sections can be determined in the same way.

Although in an ideal synthesized generalized Chebyshev filter realized in CT form, a negative cross coupling creates a TZ on the lower side and a positive cross coupling creates a TZ on the upper side of the passband [13, p. 372]; in the coupling matrix diagnosis problem, this criteria is not reliable since the filter can be badly detuned. Thus the TZs may not appear at their designed frequency point.

### C. Computer-Aided Tuning Process

Based on the extracted coupling matrix, the tuning of the DPBFs can be easily accomplished. With a suitable target coupling matrix, obtained by either a deterministic synthesis procedure or optimization, one can adjust the corresponding tuning screws aiming at reducing the difference between the extracted coupling matrix and the target coupling matrix.

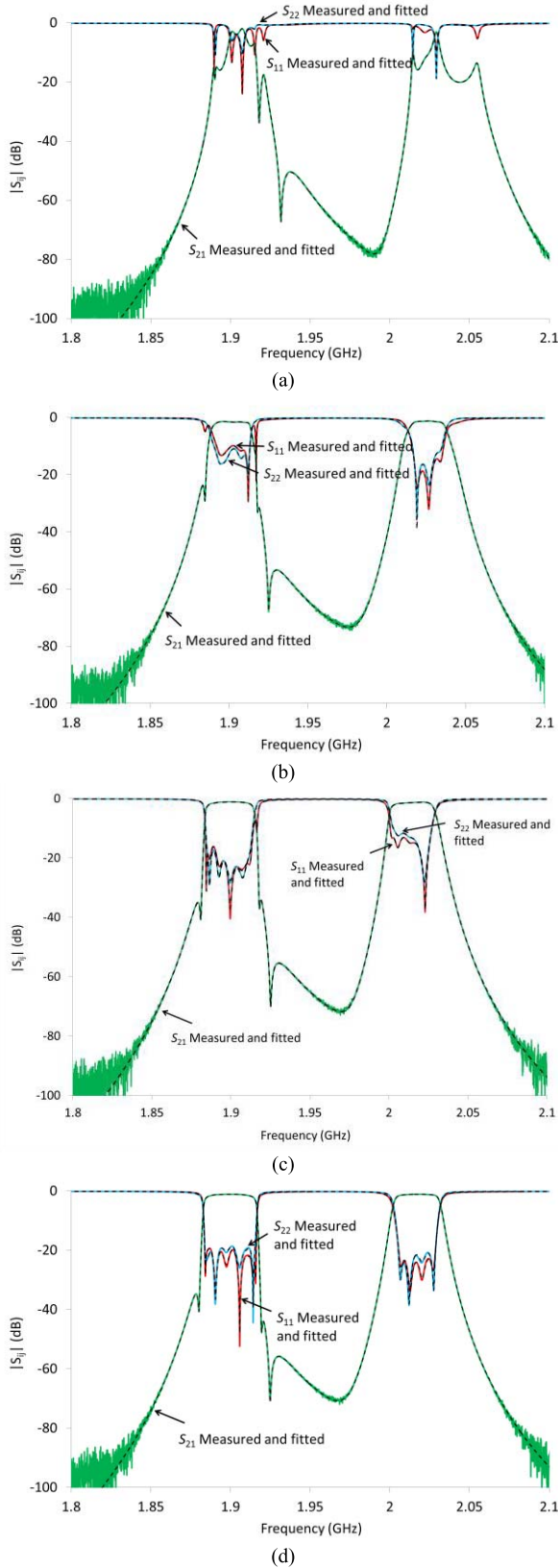


Fig. 10. Measured data and responses by extracted coupling matrices of four tuning states. Solid lines: measured data. Dashed lines: extracted coupling matrices.

Four tuning states in a complete tuning cycle of the test filter are shown in Fig. 10(a)–(d), and the real parts of the extracted coupling coefficients corresponding to the four tuning states

TABLE II  
EXTRACTED COUPLING VALUE CORRESPONDING  
TO FOUR STATES IN FIG. 10(a)–(d)

	State 1	State 2	State 3	State 4
$M_{11}$	-0.5994	-0.3047	-0.0959	-0.0953
$M_{22}$	-1.0736	-1.0740	-0.8732	-0.8729
$M_{33}$	-1.3160	-1.0429	-0.8476	-0.8755
$M_{44}$	-1.0038	-1.0044	-0.8556	-0.8798
$M_{55}$	-0.9495	-0.9488	-0.8380	-0.8766
$M_{66}$	-0.2197	-0.0094	0.0518	0.0794
$M_{77}$	0.5737	0.7251	0.7167	0.7169
$M_{88}$	0.5615	0.6547	0.6549	0.6587
$M_{99}$	0.7598	0.7600	0.7741	0.7800
$M_{10,10}$	0.7930	0.8663	0.9201	0.9305
$M_{11,11}$	0.7390	0.7390	0.7653	0.7792
$M_{12,12}$	0.6011	0.6005	0.6005	0.5797
$M_{13,13}$	-0.4731	-0.2000	-0.1269	-0.0265
$M_{14,14}$	-0.3381	0.1580	0.0834	0.0354
$M_{P1,1}$	0.7778	0.7763	0.7724	0.7725
$M_{12}$	0.3088	0.3039	0.3053	0.3048
$M_{23}$	0.1231	0.1286	0.1288	0.1282
$M_{34}$	0.1090	0.1032	0.1062	0.1064
$M_{45}$	0.1030	0.1029	0.1072	0.1083
$M_{5,14}$	0.2187	0.2251	0.2242	0.2243
$M_{16}$	0.8509	0.8475	0.8355	0.8377
$M_{67}$	0.2871	0.2858	0.2743	0.2739
$M_{78}$	0.1322	0.1313	0.1317	0.1317
$M_{89}$	0.1175	0.1161	0.1163	0.1164
$M_{9,10}$	0.0944	0.0970	0.0983	0.0985
$M_{10,11}$	0.1020	0.1027	0.1029	0.1029
$M_{11,12}$	0.0732	0.0726	0.0725	0.0721
$M_{12,13}$	0.2091	0.2087	0.2078	0.2067
$M_{13,14}$	0.8564	0.8353	0.8403	0.8420
$M_{79}$	0.0632	0.0622	0.0624	0.0625
$M_{9,11}$	-0.0771	-0.0769	-0.0768	-0.0767
$M_{11,13}$	0.1788	0.1780	0.1777	0.1773
$M_{P2,14}$	0.6506	0.6324	0.6350	0.6366
$M_{35}$	0.0024	0.0025	0.0029	0.0028
$M_{9,13}^*$	-0.0016	-0.0015	-0.0015	-0.0015
$M_{10,13}^*$	0.0021	0.0020	0.0020	0.0020

\* Stray couplings left after the proposed coupling matrix reduction scheme.

are listed in Table II. The imaginary parts of the coupling matrices are small and are not shown here. The responses of the extracted coupling matrices robustly agree with the measured data of the hardware very well.

## V. DISCUSSION

To successfully apply the proposed method to diagnose the coupling matrix, the filter is limited to a narrow to moderate bandwidth. The bandwidth counts from the lower edge of the first passband to the upper edge of the second passband. As long as preliminary tuning ensures that the resonant frequencies of the cavities are near the frequency range of interest, MVF always converges in a few iterations.

The proposed method can be applicable to low-Q filters where the imaginary parts of extracted coupling matrix count for power dissipation.

The rational fitting procedure can easily enforce stable poles during the iterations by flipping the poles on the right-half plane to the left [8]. When the method is applied to passive filters, it is found that the poles automatically appear on the left-half  $s$ -plane when MVF converges.

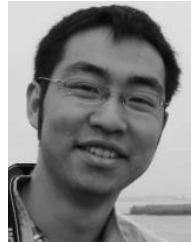
The coupling matrix transformation procedure introduced in Section III is illustrated by an ideal case where neither dispersion nor parasitic coupling is considered. When the method is used in a practical filter CAT problem, there will be additional stray couplings due to various nonideal effects, such as the dispersion and parasitic coupling effect. As illustrated in Table II, those stray couplings are marked with asterisks.

## VI. CONCLUSION

In this paper, MVF is adopted for extracting the coupling matrix of a DPBF, in which two filters are parallel connected and combined by common resonator junctions at both ends. The extraction procedure is analytical and thus is very fast as compared with optimization-based circuit model extraction techniques. A novel coupling matrix transformation procedure is proposed in this paper for the first time, which is suitable for obtaining the desired coupling matrix of a parallel-connected multiple-passband filter. Two kinds of ambiguity in the matrix similarity transformation procedure are solved in a practical and general way. It is shown that by conducting appropriate perturbations. The association of the nodes with a filter branch and that of the TZs with a particular cascaded coupling unit can be effectively determined. It is expected that the method proposed in this paper can lay a good foundation for the future robot automatic tuning of microwave resonator filters and diplexers.

## REFERENCES

- [1] M. Meng and K.-L. Wu, "An analytical approach to computer-aided diagnosis and tuning of lossy microwave coupled resonator filters," *IEEE Trans. Microw. Theory Techn.*, vol. 57, no. 12, pp. 3188–3195, Dec. 2009.
- [2] H. Hu and K.-L. Wu, "A generalized coupling matrix extraction technique for bandpass filters with uneven-Qs," *IEEE Trans. Microw. Theory Techn.*, vol. 62, no. 2, pp. 244–251, Feb. 2014.
- [3] P. Zhao and K.-L. Wu, "A new computer-aided tuning scheme for general lossy coupled-resonator bandpass filters based on the Cauchy method," *HKIE Trans.*, vol. 23, no. 1, pp. 52–62, Mar. 2016.
- [4] P. Zhao and K.-L. Wu, "Model-based vector-fitting method for circuit model extraction of coupled-resonator diplexers," *IEEE Trans. Microw. Theory Techn.*, vol. 64, no. 6, pp. 1787–1797, Jun. 2016.
- [5] G. Macchiarella and S. Tamiazzo, "Design techniques for dual-passband filters," *IEEE Trans. Microw. Theory Techn.*, vol. 53, no. 11, pp. 3265–3271, Nov. 2005.
- [6] G. Macchiarella and S. Tamiazzo, "Synthesis of dual-band filters with parallel-connected networks," in *Proc. 44th Eur. Microw. Conf.*, Oct. 2014, pp. 608–611.
- [7] H. Meng, P. Zhao, K.-L. Wu, and G. Macchiarella, "Direct synthesis of complex loaded Chebyshev filters in a complex filtering network," *IEEE Trans. Microw. Theory Techn.*, vol. 64, no. 12, pp. 4455–4462, Dec. 2016.
- [8] B. Gustavsen and A. Semlyen, "Rational approximation of frequency domain responses by vector fitting," *IEEE Trans. Power Del.*, vol. 14, no. 3, pp. 1052–1061, Jul. 1999.
- [9] R. J. Cameron, C. M. Kudsia, and R. R. Mansour, *Microwave Filters for Communication Systems: Fundamentals, Design and Applications*. Hoboken, NJ, USA: Wiley, 2007, p. 222.
- [10] S. Grivet-Talocia and B. Gustavsen, *Passive Macromodeling*. Hoboken, NJ, USA: Wiley, 2016, pp. 236–237.
- [11] D. Deschrijver, M. Mrozowski, T. Dhaene, and D. D. Zutter, "Macro-modeling of multiport systems using a fast implementation of the vector fitting method," *IEEE Microw. Wireless Compon. Lett.*, vol. 18, no. 6, pp. 383–385, Jun. 2008.
- [12] V. Mirafteb and M. Yu, "Advanced coupling matrix and admittance function synthesis techniques for dissipative microwave filters," *IEEE Trans. Microw. Theory Techn.*, vol. 57, no. 10, pp. 2429–2438, Oct. 2009.
- [13] R. J. Cameron, C. M. Kudsia, and R. Mansour, *Microwave Filters for Communication Systems: Fundamentals, Design and Applications*. Hoboken, NJ: Wiley, 2007, chs. 8–10.
- [14] V. Mirafteb and M. Yu, "Generalized lossy microwave filter coupling matrix synthesis and design using mixed technologies," *IEEE Trans. Microw. Theory Techn.*, vol. 56, no. 12, pp. 3016–3027, Dec. 2008.
- [15] S. Tamiazzo and G. Macchiarella, "An analytical technique for the synthesis of cascaded N-tuplets cross-coupled resonators microwave filters using matrix rotations," *IEEE Trans. Microw. Theory Techn.*, vol. 53, no. 5, pp. 1693–1698, May 2005.
- [16] M. Caenepeel, F. Seyfert, Y. Rolain, and M. Olivi, "Microwave filter design based on coupling topologies with multiple solutions," in *IEEE MTT-S Int. Microw. Symp. Dig.*, Phoenix, AZ, USA, May 2015, pp. 1–4.



**Ping Zhao** (S'14) received the B.Sc. degree from Nanjing University, Nanjing, China, in 2012, and the Ph.D. degree from The Chinese University of Hong Kong, Hong Kong, in 2017.

His current research interests include synthesis and computer-aided tuning algorithms for multiport microwave coupled-resonator networks, including diplexers, multiplexers and coupled-resonator decoupling networks with applications in cellular base stations and satellites.

Dr. Zhao was a recipient of Honorable Mention of the 2014 IEEE MTT-S International Microwave Symposium Student Paper Competition and the Best Transactions Paper Prize of the HKIE Transactions in 2016.



**Ke-Li Wu** (M'90–SM'96–F'11) received the B.S. and M.Eng. degrees from the Nanjing University of Science and Technology, Nanjing, China, in 1982 and 1985, respectively, and the Ph.D. degree from Laval University, Quebec, QC, Canada, in 1989.

From 1989 to 1993, he was a Research Engineer with McMaster University, Hamilton, ON, Canada. He joined the Corporate Research and Development Division, COM DEV, Cambridge, ON, in 1993, where he was a Principal Member of Technical Staff. Since 1999, he has been with The Chinese University of Hong Kong, Hong Kong, where he is currently a Professor and the Director of the Radiofrequency Radiation Research Laboratory. He has authored or co-authored numerous publications. His current research interests include EM-based circuit domain modeling of high-speed interconnections, robot automatic tuning of microwave filters, decoupling techniques of MIMO antennas, and Internet of Things technologies.

Prof. Wu is a member of the IEEE MTT-8 Subcommittee. He serves as a TPC member for many prestigious international conferences. He was an Associate Editor of the IEEE TRANSACTIONS ON MICROWAVE THEORY AND TECHNIQUES. He was a recipient of the 1998 COM DEV Achievement Award and the Asia-Pacific Microwave Conference Prize in 2008 and 2012, respectively.